COMMUNICATION

Exfoliation of triazole-based $C_3N_{4.8}$, C_3N_6, and C_3N_7 nanosheets for efficient photocatalytic ammonia production†

Ayoung Yoon,‡[a] Taehoon Kim,‡[b] Dokyung Kim,[c] Young Joo Lee, [ID][c,d] Seong-Ju Hwang [ID] *[b] and In Young Kim [ID] *[a]

Atomically thin two-dimensional nanosheets of nitrogen-rich $C_3N_{4.8}$, C_3N_6, and C_3N_7 are synthesized by sonochemical process. Despite their high nitrogen content, their triazole-based crystal structures remain intact after exfoliation. Among the present materials, the nitrogen-richest C_3N_7 nanosheets display the highest photocatalytic activity for ammonia production, highlighting the synergetic effect of composition control and exfoliation.

[a]*Department of Chemistry and Nanoscience, College of Natural Sciences, Ewha Womans University, Seoul 03760, Republic of Korea. E-mail: iykim@ewha.ac.kr*
[b]*Department of Materials Science and Engineering, College of Engineering, Yonsei University, Seoul 03722, Republic of Korea. E-mail: hwangsju@yonsei.ac.kr*
[c]*Metropolitan Seoul Center, Korea Basic Science Institute, Seoul 03759, Republic of Korea*
[d]*Department of Chemistry, Chung-Ang University, Seoul 06974, Republic of Korea*
†Electronic supplementary information (ESI) available. See DOI: https://doi.org/10.1039/d4nr03639e
‡These authors equally contributed to this work.
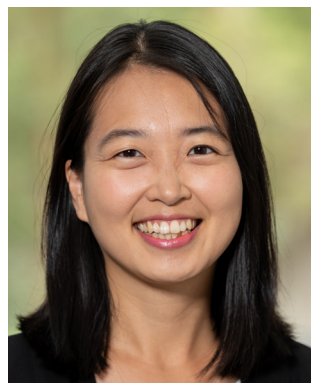
In Young Kim is an assistant professor in the Department of Chemistry and Nanoscience at Ewha Womans University (EWU). She earned her PhD (2014) at EWU. In 2017, she was awarded the prestigious ARC DECRA fellowship, which marked the beginning of her independent research career at the University of South Australia and The University of Newcastle. In 2020, she was appointed as an assistant professor at Chonnam National University before joining EWU in 2022. Her research focuses on 2D inorganic nanosheet-based nanohybrids and porous materials for energy and environmental applications, with expertise in XANES/EXAFS techniques for analyzing nanostructured materials.

In Young Kim

Although carbon nitrides of triazole-based $C_3N_{4.8}$, C_3N_6, and C_3N_7 have recently been synthesized, their inherent properties have remained largely unknown.[1] Whereas g-C_3N_4 has a heptazine-based framework,[2] the $C_3N_{4.8}$, C_3N_6, and C_3N_7 systems are stabilised through triazole frameworks together with triazine or tetrazine,[1] as indicated by density functional theory (DFT) calculations and supported by a range of techniques including X-ray diffraction (XRD), X-ray absorption spectroscopy (XAS), Fourier-transform infrared (FT-IR) spectroscopy, and transmission electron microscopy (TEM).[1] The nitrogen-rich character of carbon nitrides plays important roles in various reactions. For example, introducing nitrogen into the sp² carbon framework opens a bandgap on the carbon, enabling its use as a visible-light-sensitive g-C_3N_4 semiconductor for photocatalysis.[3] Triazole-based $C_3N_{4.8}$ shows enhanced basicity over g-C_3N_4, facilitating CO_2 feedstock reactions.[4,5] Our previous studies reported promising activities of triazole-based $C_3N_{4.8}$, C_3N_6, and C_3N_7, which outperform g-C_3N_4 in the oxygen reduction reaction (ORR)[1] and the carbon dioxide reduction reaction (CO₂RR)[5] and in applications in lithium- and sodium-ion batteries.[6] In this context, nitrogen-rich carbon nitrides have become a focus of research.[1,3–7] Triazole-based C_3N_7 is particularly noteworthy as it shows the highest nitrogen content of the carbon nitrides reported to date.

The exfoliation of g-C_3N_4 has been attempted using various strategies, including sonochemical,[8] thermal expansion,[9] intercalation,[10] and oxidation–reduction methods.[11] Exfoliated g-C_3N_4 nanosheets often exhibit enhanced performance in catalytic applications owing to their expanded surface area and changed electronic band positions.[12–14] However, exfoliation of the triazole-based $C_3N_{4.8}$, C_3N_6, and C_3N_7 has not been achieved. Because they consist of not only conjugated C–N bonds but also N–N bonds,[1] it is uncertain whether these thermodynamically unstable N–N bonds retain their integrity in triazole-based $C_3N_{4.8}$, C_3N_6, and C_3N_7 upon exfoliation.

In this study, we successfully exfoliated bulk triazole-based $C_3N_{4.8}$, C_3N_6, and C_3N_7 into nanosheets *via* a fast and efficient sonochemical process using isopropyl alcohol. XAS confirmed the retention of the triazole-based crystal structures of $C_3N_{4.8}$,

C_3N_6, and C_3N_7 upon sonochemical exfoliation. These materials have been employed as photocatalysts for nitrogen reduction reactions (NRRs). Considering the many reports on the photocatalytic NRR activities of g-C_3N_4,[15–19] triazole-based carbon nitrides provide the opportunity to enhance the NRR activities of carbon nitrides. Because the appropriate conduction band position and specific element-deficient characteristics of carbon nitrides make them suitable photocatalysts for the NRR,[18] it is important to clarify the band structures of exfoliated triazole-based $C_3N_{4.8}$, C_3N_6, and C_3N_7 nanosheets and study the relationships between their band structures and NRR properties.

The XRD patterns of bulk g-C_3N_4, $C_3N_{4.8}$, C_3N_6, and C_3N_7 are shown in Fig. S1 (see the ESI†). All samples show a strong peak between 26° and 28° corresponding to the (002) reflection of carbon nitride. As the nitrogen content in the carbon nitride increases, the (002) reflection appears at lower 2θ angles. The $d_{(002)}$ spacings of bulk g-C_3N_4, $C_3N_{4.8}$, C_3N_6, and C_3N_7 are 0.328, 0.330, 0.330, and 0.330 nm, respectively. The expansion of $d_{(002)}$ spacing is due to the repulsion of nitrogen and nitrogen.[1] For bulk g-C_3N_4, a weak peak is observed at 13°, which accounts for the in-plane reflection of the heptazine units. The peak is displaced to higher 2θ angles for bulk $C_3N_{4.8}$, C_3N_6, and C_3N_7, indicating that their core structures differ from those of bulk g-C_3N_4.

Because the XRD results do not provide information on the in-plane crystal structures of the triazole-based carbon nitrides, we analysed their structures for the first time using solid-state ^{13}C magic-angle spinning (MAS) nuclear magnetic resonance (NMR) spectroscopy. Fig. 1 shows the solid-state ^{13}C MAS NMR spectra of bulk $C_3N_{4.8}$, C_3N_6, and C_3N_7 as well as their crystal motifs together with the crystal motif of g-C_3N_4. It has been reported that g-C_3N_4 shows two well-resolved signals in the solid-state ^{13}C MAS NMR spectrum. The two signals at approximately 155 ppm and approximately 162 ppm correspond to different carbon environments, denoted as C1 and C2 in Fig. 1(b), respectively.[20,21] Interestingly, the ^{13}C NMR spectra of $C_3N_{4.8}$, C_3N_6, and C_3N_7 present broad overlapping signals that can be deconvoluted into at least three signals at 148–151, 155–158, and 161–165 ppm, as shown in Fig. 1(a).
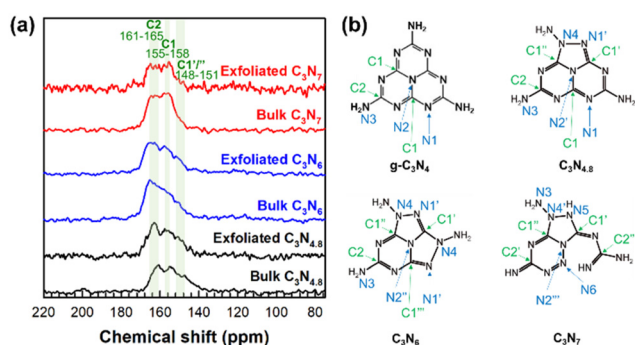
Compared to $C_3N_{4.8}$, the ^{13}C NMR signals of C_3N_6 and C_3N_7 appear at slightly higher frequencies. Interestingly, $C_3N_{4.8}$, C_3N_6, and C_3N_7 commonly display additional signals at 148–151 ppm, presumably due to the effect of the triazole motif. The relatively weakened signal at 151 ppm for C_3N_7 might be due to the altered bonding environment of carbon in the triazole motif such as the neighbouring guanidine group in C_3N_7 that is different from $C_3N_{4.8}$ and C_3N_6. Triazole exhibits ^{13}C NMR signals that are typically 20 ppm lower than those of triazine. The ^{13}C NMR spectra of the triazole-based carbon nitrides demonstrate that the in-plane crystal structures of $C_3N_{4.8}$, C_3N_6, and C_3N_7 differ, providing additional support for the crystal structures of $C_3N_{4.8}$, C_3N_6, and C_3N_7 proposed in Fig. 1(b).

Photographs of the colloidal suspensions of exfoliated nanosheets are shown in Fig. 2. The colloidal suspensions of the g-C_3N_4, $C_3N_{4.8}$, and C_3N_6 nanosheets exhibit faint ivory colours, suggesting visible-light-sensitive bandgaps. The colloidal suspension of C_3N_7 nanosheets was white, indicating a large bandgap for UV light absorption. The Tyndall phenomenon induced by exfoliated nanosheets is observed for colloidal suspensions of g-C_3N_4, $C_3N_{4.8}$, C_3N_6, and C_3N_7 nanosheets, confirming their incorporation into nanostructures. The negative zeta potential values ranging from −60 to −40 mV for the g-C_3N_4, $C_3N_{4.8}$, C_3N_6, and C_3N_7 nanosheets (Table S1, see the ESI†) demonstrate that they can form stable dispersions in isopropyl alcohol.

In terms of the crystal morphology observed by TEM, g-C_3N_4, $C_3N_{4.8}$, C_3N_6, and C_3N_7 exhibit exfoliated two-dimensional nanosheets with lateral sizes of approximately 100 nm (Fig. 3(a)). Their thicknesses are evaluated to be 0.47–0.98 nm based on their atomic force microscopy (AFM) height profile (Fig. 3(b) and (c)), which is slightly larger than the theoretical thickness of a monolayer of carbon nitrides (ca. 0.33 nm). Considering the presence of an adsorbed water layer on the surface of the carbon nitrides, it is believed that g-C_3N_4, $C_3N_{4.8}$, C_3N_6, and C_3N_7 are exfoliated into mono- or bi-layer flakes. The surface area of the exfoliated nanosheets was investigated by N_2 sorption analysis. The g-C_3N_4, $C_3N_{4.8}$, C_3N_6, and C_3N_7 nanosheets have 3–6-fold expanded Brunauer–Emmett–Teller (BET) surface area as compared to their parent bulk materials (Fig. S2, see the ESI†). The expanded surface area and better N_2 adsorption ability of exfoliated carbon nitride nanosheets could contribute to increased catalytic performance of g-C_3N_4, $C_3N_{4.8}$, C_3N_6, and C_3N_7 upon exfoliation.

Fig. 1 (a) Solid-state ^{13}C MAS NMR spectra of bulk and exfoliated $C_3N_{4.8}$, C_3N_6, and C_3N_7. (b) Crystal motifs of g-C_3N_4, $C_3N_{4.8}$, C_3N_6, and C_3N_7.
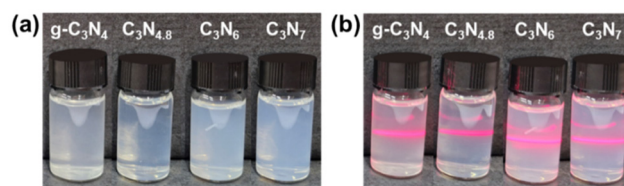

Fig. 2 (a) Photographs and (b) Tyndall phenomenon of colloidal suspensions of exfoliated g-C_3N_4, $C_3N_{4.8}$, C_3N_6, and C_3N_7 nanosheets.
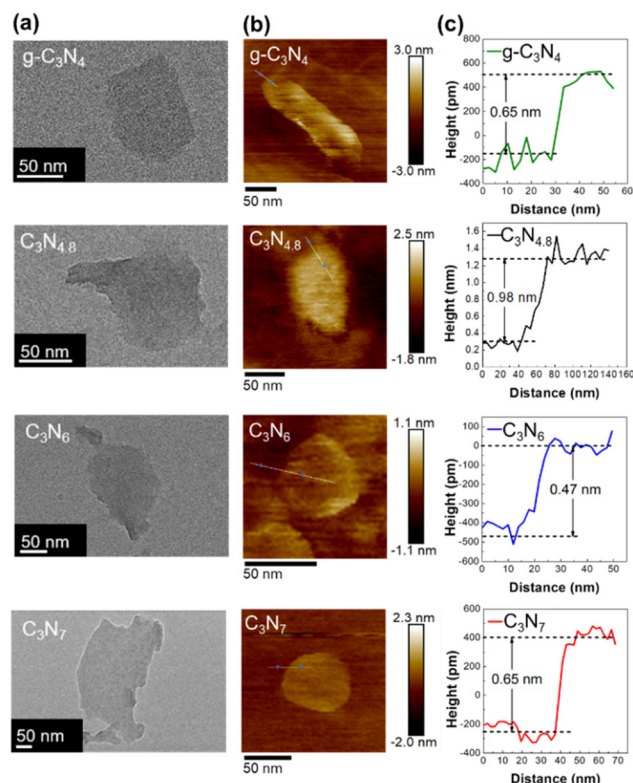
Fig. 3 (a) TEM and (b) AFM images and (c) height profiles for exfoliated g-C_3N_4, $C_3N_{4.8}$, C_3N_6, and C_3N_7 nanosheets.

Fig. 4 (a) N 1s XPS spectra and (b) (left) C K- and (right) N K-edge NEXAFS spectra of exfoliated g-C_3N_4, $C_3N_{4.8}$, C_3N_6, and C_3N_7 nanosheets.

The structural retention of triazole-based carbon nitrides upon exfoliation are confirmed by solid-state ^{13}C MAS NMR spectroscopy as shown in Fig. 1(a). The ^{13}C MAS NMR spectral features of exfoliated $C_3N_{4.8}$, C_3N_6, and C_3N_7 nanosheets are identical to those of their parent bulk materials. X-ray photoelectron spectroscopy (XPS) analysis results also support the structural retention of the triazole-based carbon nitrides after exfoliation. The C 1s and N 1s XPS spectra of the exfoliated g-C_3N_4, $C_3N_{4.8}$, C_3N_6, and C_3N_7 nanosheets are shown in Fig. S3† and Fig. 4(a), respectively. The overall N 1s XPS spectral features of the exfoliated $C_3N_{4.8}$, C_3N_6, and C_3N_7 nanosheets are the same as the XPS spectral features of bulk $C_3N_{4.8}$, C_3N_6, and C_3N_7 (Fig. S4, see the ESI†), indicating a retention of the triazole-based structure after exfoliation. In both bulk and exfoliated nanosheet systems, g-C_3N_4 samples display an intense binding energy of C–N=C (N1) and a weaker binding energy of N–(C)$_3$ (N2), which are typical N 1s XPS spectral features of g-C_3N_4.[24,25] In contrast, exfoliated $C_3N_{4.8}$, C_3N_6, and C_3N_7 nanosheets and their bulk samples have an additional component at a binding energy of approximately 400.0 eV in their N 1s XPS spectra, which correspond to the binding energy of N–N (N4) in the triazole-based structure. The terminal N–H$_2$ (N3) feature at approximately 404.6 eV is weak or negligible in N 1s XPS spectra of all present carbon nitride samples due to their low portion in materials.

Detailed local atomic structures of exfoliated g-C_3N_4, $C_3N_{4.8}$, C_3N_6, and C_3N_7 nanosheets were further examined *via*

near-edge X-ray absorption fine structure (NEXAFS) analysis at the C K- and N K-edges (Fig. 4(b)). In the C K-edge spectra, the g-C_3N_4 nanosheets show π^* excitations from the C=C plane, HN–C=N (C2), and N–C=N (C1) at 285.2, 287.3, and 288.0 eV, respectively.[22,23] While the π^* positions of C=C for g-C_3N_4 and triazole-based $C_3N_{4.8}$, C_3N_6, and C_3N_7 nanosheets are the same, the triazole-based $C_3N_{4.8}$, C_3N_6, and C_3N_7 nanosheets exhibit π^* of N–C=N (C1′ and C1″) at higher energy compared to g-C_3N_4. The π^* blueshift of N–C=N (C1) is an intrinsic spectral feature for triazole-based carbon nitrides, which arises from reinforcement of N–C=N (C1′ and C1″) by neighbouring N–N (N4) bonds.[1] In the N K-edge spectra, unlike g-C_3N_4 nanosheets, the triazole-based $C_3N_{4.8}$, C_3N_6, and C_3N_7 nanosheets display π^* of heterocyclic N–N (N4) bonds at 400.2 eV. This is an additional unique spectral feature of triazole-based carbon nitrides, which is associated with the emergence of the N–N (N4) component at a binding energy of approximately 400.0 eV in the N 1s XPS spectra of triazole-based $C_3N_{4.8}$, C_3N_6, and C_3N_7 samples. The C K- and N K-edge NEXAFS spectral features of exfoliated $C_3N_{4.8}$, C_3N_6, and C_3N_7 nanosheets are in good agreement with those of highly

ordered mesoporous $C_3N_{4.8}$, C_3N_6, and C_3N_7 reported previously,[1] highlighting that all the triazole-based materials maintained their crystal structure after exfoliation into nanosheets.

The spectroscopic analyses support the conclusion that the triazole-based atomic structures of $C_3N_{4.8}$, C_3N_6, and C_3N_7 remain unchanged after the sonochemical process, which is contrary to the general expectation that nitrogen-rich compounds can easily decompose under high external energy.[26] When additional TEM analyses were conducted to confirm whether the nitrogen-rich triazole-based $C_3N_{4.8}$, C_3N_6, and C_3N_7 nanosheets decomposed or were retained, the exfoliated $C_3N_{4.8}$, C_3N_6, and C_3N_7 nanosheets maintained the nanosheet morphology after 30 d in isopropyl alcohol, indicating their excellent long-term stability (Fig. S5, see the ESI†).

Because band structural features, including the bandgap and band position, are critical for carbon nitrides as photocatalysts,[27] the band structures of the triazole-based $C_3N_{4.8}$, C_3N_6, and C_3N_7 nanosheets were examined by UV–Vis spectroscopy and ultraviolet photoelectron spectroscopy (UPS). As shown in Fig. 5(a), the bandgaps of the triazole-based $C_3N_{4.8}$, C_3N_6, and C_3N_7 nanosheets increased upon exfoliation, with bulk g-C_3N_4, $C_3N_{4.8}$, C_3N_6, and C_3N_7 having optical bandgaps of 2.63, 2.00, 2.70, and 3.00 eV, respectively. The optical bandgaps of g-C_3N_4, $C_3N_{4.8}$, C_3N_6, and C_3N_7 nanosheets were 2.72, 2.26, 2.84, and 3.18 eV, respectively. All the exfoliated nanosheets show visible-light absorption below the band edge termed the Urbach tail owing to their low crystallinity.[28] The UPS provides information on the top position of the valence bands of carbon nitrides.[29] Based on the UPS spectra of the triazole-based $C_3N_{4.8}$, C_3N_6, and C_3N_7 nanosheets plotted in Fig. 5(b), the band structures of the corresponding nanosheets are shown in Fig. 5(c). Their valence band top position does not significantly differ from that of the g-C_3N_4 nanosheet in the range of 1.80–1.90 eV $vs.$ NHE;[29] however, the conduction band position shifts toward negative potentials as the nitrogen content increases for the triazole-based carbon nitrides. The conduction band positions of triazole-based $C_3N_{4.8}$, C_3N_6, and C_3N_7 nanosheets are −0.36, −0.94, and −1.38 eV $vs.$ NHE, respectively. As compared to g-C_3N_4 nanosheets, triazole-based C_3N_7 nanosheets have a more negative conduction band position, indicating higher potential energy to reduce nitrogen to ammonia at 0.55 eV $vs.$ NHE.[30] This characteristic of C_3N_7 nanosheets could help lower the activation energy of N_2 for the NRR.

Prior to examining the photocatalytic NRR activities of the triazole-based nanosheets, those of bulk carbon nitrides were investigated. The NRR performances of bulk g-C_3N_4, $C_3N_{4.8}$, C_3N_6, and C_3N_7 are shown in Fig. S6 (see the ESI†). Bulk C_3N_7 exhibits the highest activity for ammonia production, underscoring the usefulness of nitrogen enrichment in improving the NRR activity of carbon nitride. As presented in Fig. 6(a), all present carbon nitride materials commonly show a significant improvement of photocatalyst performance upon exfoliation. Based on N_2 sorption analysis, the improvement in the NRR activity upon exfoliation is ascribed to enhanced N_2 adsorption
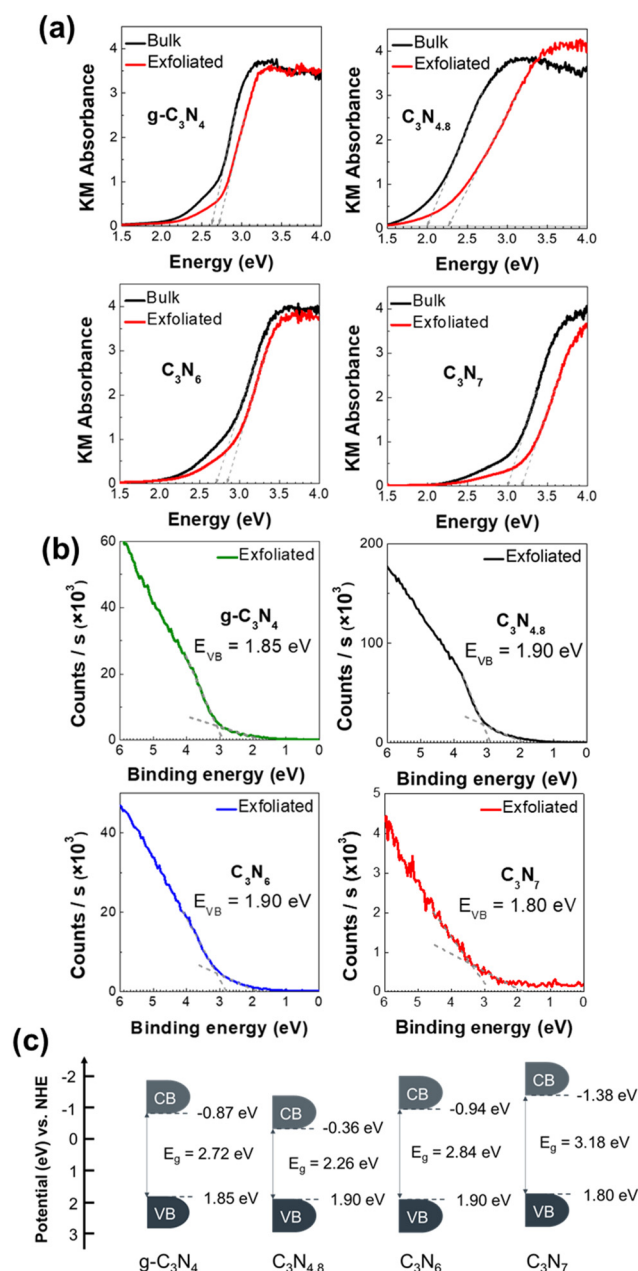

Fig. 5 (a) UV–Vis absorption spectra, (b) UPS spectra, and (c) schematic illustration of the band position for exfoliated g-C_3N_4, $C_3N_{4.8}$, C_3N_6, and C_3N_7 nanosheets.

efficiency on the expanded surface of exfoliated nanosheets of carbon nitrides. The ammonia production rates of exfoliated g-C_3N_4, $C_3N_{4.8}$, C_3N_6, and C_3N_7 nanosheets are approximately 242.1, 60.8, 265.8, and 472.4 μmol g_{cat}^{-1} h^{-1}, respectively. In the triazole-based carbon nitride system, the ammonia production rates are enhanced as the nitrogen content in carbon nitride increases. Furthermore, triazole-based C_3N_6 and C_3N_7 nanosheets outperform exfoliated g-C_3N_4 nanosheets as catalysts for the photocatalytic NRR. These results highlight the importance of the nitrogen-enrichment of triazole-based carbon nitrides in developing efficient NRR photocatalysts.
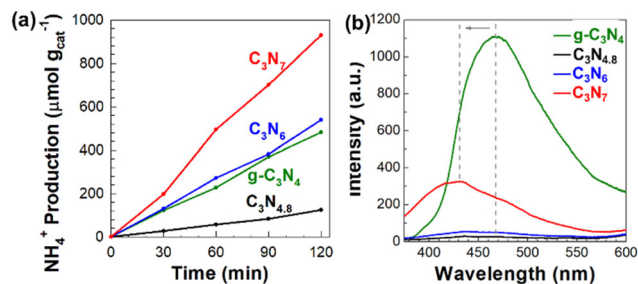
Fig. 6 (a) Amount of generated ammonia under a N_2 atmosphere and (b) PL spectra for exfoliated g-C_3N_4, $C_3N_{4.8}$, C_3N_6 and C_3N_7 nanosheets.

The NRR performance of carbon nitride increases in the order of $C_3N_{4.8} <$ g-$C_3N_4 < C_3N_6 < C_3N_7$ in both bulk and exfoliated nanosheet systems, which is an inverse trend with an expectation on NRR performance based on the bandgap size of photocatalysts. Generally, it is expected that a broader bandgap results in reduced photocatalytic performance owing to the reduced light harvesting ability.[31] Our opposite observation to the expectation indicates that light harvest ability is not the most critical factor affecting NRR performance in the present triazole-based carbon nitrides system.

The other affecting factors for the NRR performance of carbon nitride catalysts are their surface area and N_2 adsorption efficiency. Given that the NRR performance of g-C_3N_4 nanosheets with the largest surface area is lower than those of triazole-based C_3N_6 and C_3N_7 nanosheets, the surface area and N_2 adsorption efficiency are not the primary factors for the NRR.

The increasing NRR performance trend in the order of $C_3N_{4.8} <$ g-$C_3N_4 < C_3N_6 < C_3N_7$ nanosheets is exactly matched with the more negative conduction band position trend of $C_3N_{4.8}$, g-C_3N_4, C_3N_6, and C_3N_7 nanosheets. This good agreement strongly demonstrates that carbon nitride nanosheets with a more negative conduction band position exhibit better NRR activity due to their higher potential energy to reduce nitrogen to ammonia at 0.55 eV *vs.* NHE.

We also investigated the charge recombination behaviour of all exfoliated carbon nitride nanosheets by photoluminescence (PL) spectroscopy. In general, the low photocatalytic activity of g-C_3N_4 nanosheets is due to their rapid charge recombination.[32,33] As shown in Fig. 6(b), the g-C_3N_4 nanosheets display a strong PL signal at 468.6 nm, suggesting significant charge recombination. In contrast, triazole-based $C_3N_{4.8}$, C_3N_6, and C_3N_7 nanosheets exhibit either negligible or very depressed PL signals, highlighting good charge separation within them. Compared to g-C_3N_4 nanosheets, the C_3N_7 nanosheets represent a blue-shifted PL at 432.2 nm, which is associated with their bandgap broadening. In addition to the optimization effect of the conduction band position, the efficient charge separation in the C_3N_7 nanosheets evidenced by their weak PL signal synergistically contributes towards enhancing their photocatalytic NRR performance.

As present carbon nitrides are nitrogen-rich, cautious ammonia quantification is required when using them as a photocatalyst in the NRR.[34–36] To confirm that the present carbon nitride nanosheets are not decomposed to contribute to ammonia production, the photocatalytic NRR under an Ar atmosphere and cyclability test of a photocatalyst were performed for triazole-based C_3N_7 nanosheets. As shown in Fig. S7 of the ESI,† negligible ammonia production on C_3N_7 nanosheets under an Ar atmosphere obviously demonstrates the fixation of atmospheric N_2 into ammonia on the C_3N_7 nanosheets. The excellent photocatalytic stability of the C_3N_7 nanosheets is confirmed by the consecutive NRR activity test, showing no significant degradation in the continuous 5 cycles; see Fig. S8 of the ESI.†

Conclusions

We developed a sonochemical exfoliating process for triazole-based $C_3N_{4.8}$, C_3N_6, and C_3N_7 nanosheets with thicknesses of 0.47–0.98 nm. The crystal structures and band structures of the triazole-based $C_3N_{4.8}$, C_3N_6, and C_3N_7 nanosheets were revealed by systematic spectroscopic analyses. The exfoliated triazole-based $C_3N_{4.8}$, C_3N_6, and C_3N_7 nanosheets retain the parent triazole-based crystal structures and possess more negative conduction band positions with respect to the reduction potential of N_2 to NH_3 (0.55 V *vs.* NHE at pH 0), while their valence band positions do not differ significantly. The NRR performance of the carbon nitrides increases in the order of $C_3N_{4.8} <$ g-$C_3N_4 < C_3N_6 < C_3N_7$ in both bulk and exfoliated nanosheet systems, which is exactly matched with the conduction band position trend of g-C_3N_4, $C_3N_{4.8}$, C_3N_6, and C_3N_7 nanosheets. Additionally, PL analysis of all present carbon nitride nanosheets shows that charge recombination is alleviated within triazole-based carbon nitride nanosheets rather than g-C_3N_4 nanosheets. Given all these factors, it is concluded that the optimized conduction band position and suppressed charge recombination make triazole-based C_3N_7 nanosheets the best catalyst in the photocatalytic NRR. The nitrogen-richest C_3N_7 nanosheets highlight the high efficacy of the simultaneous composition control and exfoliation approach for optimising the photocatalytic activity of triazole-based carbon nitrides.

Author contributions

A. Y.: investigation, visualisation, and writing – original draft; T. K.: investigation and formal analysis; D. K.: investigation and formal analysis; Y. J. L.: methodology and writing – review and editing; S.-J. H.: conceptualisation, methodology, writing – review and editing, and funding acquisition; I. Y. K.: supervision, conceptualisation, writing – review and editing, and funding acquisition.

Data availability

The data supporting this article have been included as part of the ESI.†

Conflicts of interest

There are no conflicts to declare.

Acknowledgements

References

1 I. Y. Kim, S. Kim, S. Premkumar, J.-H. Yang, S. Umapathy and A. Vinu, *Small*, 2020, **16**, 1903572.

2 S. Lee, E. Y. Shin, D. Jang, S. Choi, H. Park, J. Kim and S. Park, *Bull. Korean Chem. Soc.*, 2022, **43**, 1124.

3 G. R. Dillip, T. V. M. Sreekanth and S. W. Joo, *Ceram. Int.*, 2017, **43**, 6437.

4 P. Kumar, E. Vahidzadeh, U. K. Thakur, P. Kar, K. M. Alam, A. Goswami, N. Mahdi, K. Cui, G. M. Bernard, V. K. Michaelis and K. Shankar, *J. Am. Chem. Soc.*, 2019, **141**, 5415.

5 S. Kim, G. Singh, C. Sathish, P. Panigrahi, R. Daiyan, X. Lu, Y. Sugi, I. Y. Kim and A. Vinu, *Chem. – Asian J.*, 2021, **16**, 3999.

6 S. Kim, M. Hankel, W. Cha, G. Singh, J. M. Lee, I. Y. Kim and A. Vinu, *Nano Energy*, 2020, **72**, 104702.

7 S. M. Ruban, C. I. Sathish, K. Ramadass, S. Joseph, S. Kim, V. D. B. C. Dasireddy, I. Y. Kim, A. H. Al-Muhtaseb, Y. Sugi and A. Vinu, *ChemCatChem*, 2021, **13**, 468.

8 W. Wang, G. Li, T. An, D. K. L. Chan, J. C. Yu and P. K. Wong, *Appl. Catal., B*, 2018, **238**, 126.

9 L. Yang, X. Liu, Z. Liu, C. Wang, G. Liu, Q. Li and X. Feng, *Ceram. Int.*, 2018, **44**, 20613.

10 C. Hu, W.-F. Tsai, W.-H. Wei, K.-Y. A. Lin, M.-T. Liu and K. Nakagawa, *Carbon*, 2021, **175**, 467.

11 P. Xia, B. Zhu, B. Cheng, J. Yu and J. Xu, *ACS Sustainable Chem. Eng.*, 2018, **6**, 965.

12 C. Wu, S. Xue, Z. Qin, M. Nazari, G. Yang, S. Yue, T. Tong, H. Ghasemi, F. C. R. Hernandez, S. Xue, D. Zhang, H. Wang, Z. M. Wang, S. Pu and J. Bao, *Appl. Catal., B*, 2021, **282**, 119557.

13 X. Wu, X. Wang, F. Wang and H. Yu, *Appl. Catal., B*, 2019, **247**, 70.

14 Y. Li, M. Yang, Y. Xing, X. Liu, Y. Yang, X. Wang and S. Song, *Small*, 2017, **13**, 1701552.

15 N. H. Kwon, J. Park, X. Jin, S.-J. Kim, H. Kim and S.-J. Hwang, *ACS Nano*, 2023, **17**, 23732.

16 N. H. Kwon, S.-J. Shin, X. Jin, Y. Jung, G.-S. Hwang, H. Kim and S.-J. Hwang, *Appl. Catal., B*, 2020, **277**, 119191.

17 G. Liu, Z. Tang, X. Gu, N. Li, H. Lv, Y. Huang, Y. Zeng, M. Yuan, Q. Meng, Y. Zhou and C. Wang, *Appl. Catal., B*, 2022, **317**, 121752.

18 G. Dong, W. Ho and C. Wang, *J. Mater. Chem. A*, 2015, **3**, 23435.

19 Y. Xue, Y. Guo, Z. Liang, H. Cui and J. Tian, *J. Colloid Interface Sci.*, 2019, **556**, 206.

20 W. Li, Z. Guo, L. Jiang, L. Zhong, G. Li, J. Zhang, K. Fan, S. Gonzalez-Cortes, K. Jin, C. Xu, T. Xiao and P. P. Edwards, *Chem. Sci.*, 2020, **11**, 2716.

21 D. Vidyasagar, S. G. Ghugal, S. S. Umare and M. Banavoth, *Sci. Rep.*, 2019, **9**, 7186.

22 I. Y. Kim, S. Kim, X. Jin, S. Premkumar, G. Chandra, N.-S. Lee, G. P. Mane, S.-J. Hwang, S. Umapathy and A. Vinu, *Angew. Chem., Int. Ed.*, 2018, **57**, 17135.

23 Y. Zheng, Y. Jiao, Y. Zhu, L. H. Li, Y. Han, Y. Chen, A. Du, M. Jaroniec and S. Z. Qiao, *Nat. Commun.*, 2014, **5**, 3783.

24 K. Akaike, K. Aoyama, S. Dekubo, A. Onishi and K. Kanai, *Chem. Mater.*, 2018, **30**, 2341.

25 S. Gu, J. Xie and C. M. Li, *RSC Adv.*, 2014, **4**, 59436.

26 W. Sun, A. Holder, B. Orvañanos, E. Arca, A. Zakutayev, S. Lany and G. Ceder, *Chem. Mater.*, 2017, **29**, 6936.

27 D. Zhao, C.-L. Dong, B. Wang, C. Chen, Y.-C. Huang, Z. Diao, S. Li, L. Guo and S. Shen, *Adv. Mater.*, 2019, **31**, 1903545.

28 K. J. Archana, A. C. Preetha and K. Balasubramanian, *Opt. Mater.*, 2022, **127**, 112245.

29 Y. Kang, Y. Yang, L.-C. Yin, X. Kang, G. Liu and H.-M. Cheng, *Adv. Mater.*, 2015, **27**, 4572.

30 Y. Huang, N. Zhang, Z. Wu and X. Xie, *J. Mater. Chem. A*, 2020, **8**, 4978.

31 B. S. Reghunath, S. Rajasekaran, S. Mathew, D. Pinheiro, S. Devi K. R, S. Jung, T. Jayaraman and M. Y. Choi, *Bull. Korean Chem. Soc.*, 2023, **44**, 969.

32 S. Choe, S. M. Kim, Y. Lee, J. Seok, J. Jung, J. S. Lee and Y. J. Jang, *Nano Convergence*, 2021, **8**, 22.

33 C. Liang, H. Y. Niu, H. Guo, C. G. Niu, D. W. Huang, Y. Y. Yang, H. Y. Liu, B. B. Shao and H. P. Feng, *Chem. Eng. J.*, 2020, **396**, 125395.

34 Y. Zhao, R. Shi, X. Bian, C. Zhou, Y. Zhao, S. Zhang, F. Wu, G. I. N. Waterhouse, L.-Z. Wu, C.-H. Tung and T. Zhang, *Adv. Sci.*, 2019, **6**, 1802109.

35 D. Li, Y. Zhao, Y. Miao, C. Zhou, L.-P. Zhang, L.-Z. Wu and T. Zhang, *Adv. Mater.*, 2022, **34**, 2207793.

36 A. C. Nielander, J. M. McEnaney, J. A. Schwalbe, J. G. Baker, S. J. Blair, L. Wang, J. G. Pelton, S. Z. Andersen, K. Enemark-Rasmussen, V. Čolić, S. Yang, S. F. Bent, M. Cargnello, J. Kibsgaard, P. C. K. Vesborg, I. Chorkendorff and T. F. Jaramillo, *ACS Catal.*, 2019, **9**, 5795.